**Journal of**

**Applied and Computational Mechanics**

Shahid Chamran
University of Ahvaz

Research Paper

# Even and Uneven Porosities on Rotating Functionally Graded Variable-thickness Annular Disks with Magneto-electro-thermo-mechanical Loadings

## Rania Tantawy[1], Ashraf M. Zenkour[2]

[1] Department of Mathematics, Faculty of Science, Damietta University, P.O. Box 34517, Egypt, Email: rania_eltantwy@yahoo.com
[2] Department of Mathematics, Faculty of Science, Kafrelsheikh University, Kafrelsheikh 33516, Egypt, Email: zenkour@sci.kfs.edu.eg

**Abstract.** This paper investigates the porosity effect on rotating functionally graded piezoelectric (FGP) variable-thickness annular disk. Even and uneven porosity distributions for the disk are approximated. The porous annular disk is subjected to the influence of electromagnetic, thermal, and mechanical loadings. Material coefficients are graded and described as a power law in the radial direction of the annular rotating disk. The resulting differential equation with boundary conditions is solved using the semi-analytical technique. Two cases are studied for the porous annular disk, circular disk, and mounted disk. The effectiveness of the porosity factor and grading index on the temperature, stresses, and displacement are reported. Comparisons between non-porous and porous annular disks for even and uneven porosity are executed and discussed. The obtained results are presented to conclude the important role of porosity on the rotating variable-thickness annular disk for the purpose of engineering mechanical design.

**Keywords:** Even and uneven distributions; hollow disk; uniform magnetic field; thermal loading; piezoelectric material.

## 1. Introduction

Nowadays, due to the progress in manufacturing of advanced materials, the functionally graded porosity can be presented as one of the latest progress in functionally graded materials (FGMs). Low density, flexibility engineering structures, and temperature stability are among the most important features of porous materials. These advantages have attracted many experiments and engineering applications on advanced structures made of porous materials. Functionally graded porous materials are used to produce smart structures in the automotive industry, aerospace, military operations, shipbuilding, biomedical, and more modern engineering structures. Many researchers have introduced papers to study the mechanical, electrical, and thermal effects on porous structures and compare them with those of non-porous materials.

Some researchers are also concerned with even, uneven, and other porosity distributions. Abazid et al. [1] studied wave propagation by using strain gradient theory in porous functionally graded graphene platelets with mechanical and magnetic loads. Free vibration analysis for porous electro-magneto-elastic functionally graded plates was investigated by Ebrahimi et al. [2]. Porosity distribution is supposed in even and uneven form. Arefi et al. [3] presented porous FG graphene nanoplatelets with a transverse load. Barati and Shahverdi [4] presented porosity-dependent hygro- aero-thermal of FGM panels. Random porosity is investigated in even and uneven porosity types. Sobhy and Zenkour [5] displayed wave propagation in bilayer FG porous nanoplates in a magnetic field by using a quasi-3D refined plate theory. Vaka et al. [6] offered a dynamic analysis of a non-uniform porous (FG) rotor-bearing system by the finite element method. Kumar and Panchal [7] introduced plane wave propagation in a porous half-space placed in a stationary magnetic field. Kumar and Sharma [8] analyzed porous magneto-piezo-thermoelastic governing equations for an anisotropic medium. Karami et al. [9] have presented wave propagation in nanoplate porous FGMs placed in the magnetic field. Kiran et al. [10] studied the porosity effect on FG skew electro-magneto-elastic plates by using a finite element method. Wattanasakulpong and Ungbhakorn [11] have shown a survey on the vibration of FG porous beams with different boundary conditions by differential transformation technique. Akbas [12] analyzed the vibrations of porous FG deep beams under thermal loading with even and uneven porosity images. Chen et al. [13] discussed the nonlinear vibration on porous Timoshenko FG sandwich beams for various distributions of porosity. Ebrahimi and Jafari [14] presented the vibration on a porous FG Reddy beam with even and uneven distributions of porosity. Tantawy and Zenkour [15] introduced a porous FGP hollow sphere. The sphere is under various mechanical and thermal loading in a hygrothermal environment. Zenkour [16] investigated porous FG thick rectangular plates using a higher-order shear deformation theory. Mashat et al. [17] presented a survey on the effect of temperature and moisture on porous FG plates resting on elastic foundations. There are several papers about the effects of porosity distribution on the mechanical response of structures such as [18-22]. There are also many papers studying the mechanical response of circular

or annular plates [23, 24].

Two types of non-uniform porosity distribution are concerned in this paper. Consider the porosity distribution in even and uneven forms. The paper presents various loading on a rotating porous, functionally graded, piezoelectric annular disk. The magneto-electric effect, thermal distribution, and mechanical loading on the internal and external radius have occurred. Physical material coefficients are varying through the thickness as a power law in the radius direction. Firstly, solve the electrostatic equation with the aid of Maxwell's equations of electrodynamics, and then solve the heat equation and equilibrium equation by using the semi-analytical solutions. Numerical results study the presence effect of porosity for perfect and porous materials in two cases for even and uneven porosities are presented.

## 2. Geometric Profile of the Disk

Let us consider a thin axisymmetric functionally graded (FG) annular disk with variable thickness. The disk is presented in power or exponential form with an inner radius $a$ and outer radius $b$. The functionally graded disk is rotating with angular velocity $\omega$. The cylindrical coordinates $(r, \theta, z)$ are used according to the disk profiles. The internal surface of the disk is made of PZT-4 while the external surface is made of Cadmium Selenide. Between the two surfaces, the porous material is graded according to the power function in the radius direction. Even and uneven non-uniform porosity distribution is considered. The porous disk is affected by mechanical pressure, thermal distribution, electric potential, and stationary magnetic field.

### 2.1 Thickness description

The disk thickness description is assumed in a power-law type [27, 28]:

$$h(r) = h_0[1 - l(\tfrac{r}{b})]^k, \tag{1}$$

where $h_0$ indicates the thickness at the center of the disk, $k$, and $l$ are geometric coefficients. Coefficient $k$ determines the disk appearance: at $k = 1$ the disk has a linearly decreasing thickness. The disk has a concave profile for $l < 1$ while it has a convex profile for $l > 1$. Various profiles of the disk are shown in Figure 1.
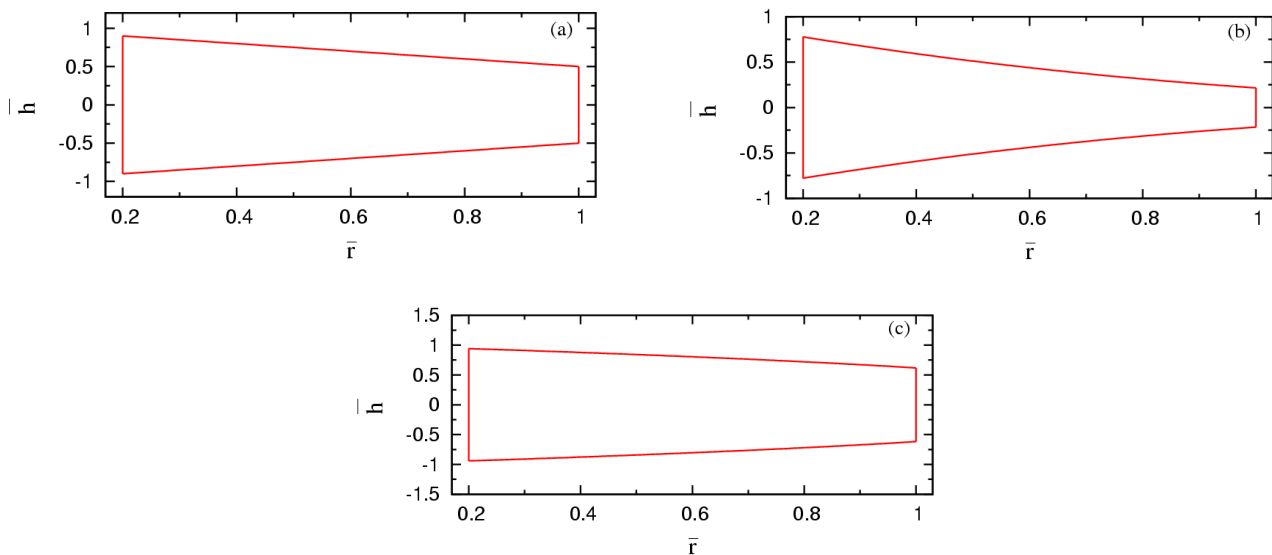


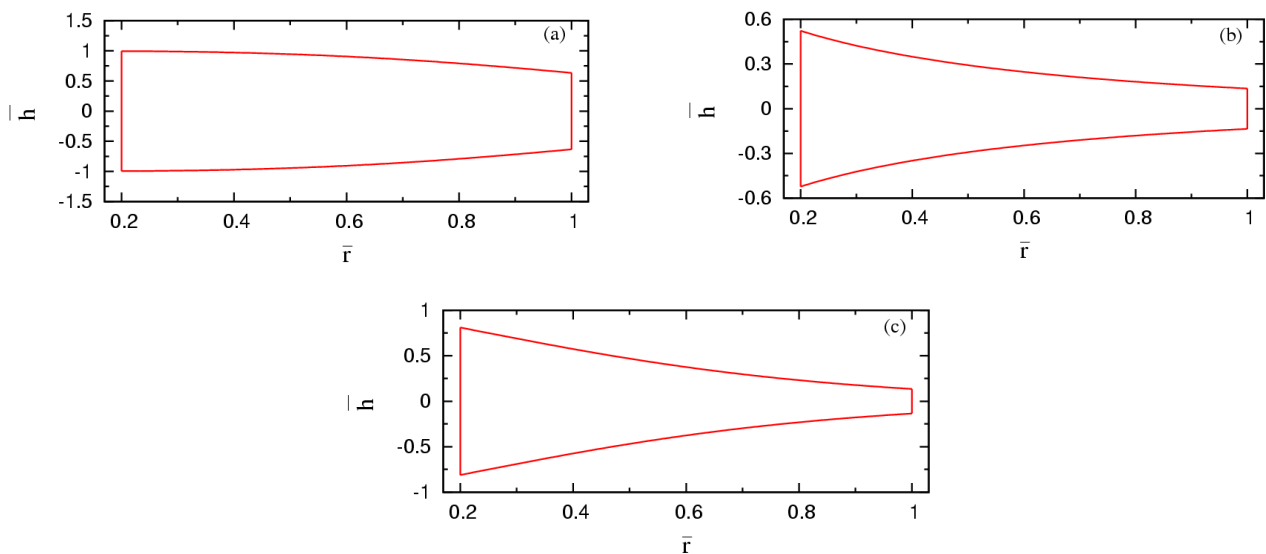**Fig. 1.** Thickness description of FG annular disk (a) linear, (b) convex and (c) concave shapes.



**Fig. 2.** The thickness profile of FG annular disk in an exponential form for (a) $l = 0.4568, k = 3$, (b) $l = 2, k = 0.7$, (c) $l = 2, k = 1.4$.
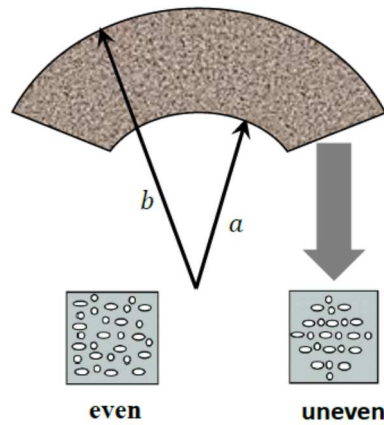
**Fig. 3.** Configuration of the annular disk with porosity distribution.

Another thickness type of the disk description is the exponential form [29]:

$$h(r) = h_0 e^{-l(\frac{r}{b})^k}, \tag{2}$$

where $l$ determines the edge thickness of the disk and $k$ defines the disk shape profile. The disk profiles in the exponential form are plotted in Figure2.

### 2.2 Porosity distribution description

Suppose that the rotating FG annular disk with two types of porosity distributions, even and uneven porosities as shown in Figure 3. The physical material coefficients of the annular disk are expressed by the modified power function $p(r)$ [6]:

$$p(r) = \begin{cases} (p^{(b)} - p^{(a)}) \left(\frac{r-a}{b-a}\right)^n + p^{(a)} - (p^{(a)} + p^{(b)}) \left(1 - \frac{r}{b}\right) \frac{\beta}{2} & even\ porosity, \\ (p^{(b)} - p^{(a)}) \left(\frac{r-a}{b-a}\right)^n + p^{(a)} - (p^{(a)} + p^{(b)}) \left(\frac{r}{b}\right) \frac{\beta}{2} & uneven\ porosity. \end{cases} \tag{3}$$

where $n \geq 0$ describes the material grading index, $p^{(a)}$, $p^{(b)}$ are corresponding to the physical material characteristics of internal and external surfaces and $0 \leq \beta \leq 1$ is the porosity parameter. For non-porous material, we can easily set $\beta = 0$.

### 2.3 Thermal distribution properties

The temperature equation of the annular porous disk can be expressed in the form [29, 30]:

$$\frac{1}{rh(r)} \frac{d}{dr} \left[ r\ k_T\ h(r) \frac{dT(r)}{dr} \right] = 0 \tag{4}$$

where $k_T$ is the heat conductivity parameter which obeys the graded relations (3).

The temperature boundary conditions are considered in the form:

$$T(r)|_{r=a} = T_0, \quad T(r)|_{r=b} = T_1, \tag{5}$$

where $T_0$ is the reference initial temperature and $T_1$ is the temperature value at the external surface.

## 3. Magneto-elastic Differential Equations

The mathematical constitutive equations for porous FG annular rotating variable thickness disks with mechanical, thermal, and electric loading can be written in the form [31-33]:

$$\begin{Bmatrix} \sigma_r \\ \sigma_\theta \end{Bmatrix} = \begin{bmatrix} c_{rr} & c_{r\theta} & e_{rr} \\ c_{r\theta} & c_{\theta\theta} & e_{r\theta} \end{bmatrix} \begin{Bmatrix} \frac{du}{dr} \\ \frac{u}{r} \\ \frac{d\psi}{dr} \end{Bmatrix} - \begin{Bmatrix} \lambda_r \\ \lambda_\theta \end{Bmatrix} T(r), \tag{6}$$

while electric displacement is:

$$D_r = e_{rr} \frac{du}{dr} + e_{r\theta} \frac{u}{r} - \varepsilon_{rr} \frac{d\psi}{dr} + p_{11} T(r), \tag{7}$$

where $c_{ij}$ $(i, j = r, \theta, z)$, $e_{rj}$ $(j = r, \theta)$, $\varepsilon_{rr}$, and $p_{11}$ denote the elastic, piezoelectric, dielectric, and pyroelectric coefficients, and:

$$\lambda_r = c_{rr}\alpha_r + c_{r\theta}\alpha_\theta, \quad \lambda_\theta = c_{r\theta}\alpha_r + c_{\theta\theta}\alpha_\theta, \tag{8}$$

where $\alpha_i$ are the thermal expansion parameters.

Suppose that the magnetic permeability $\mu(r)$ of the disk are identical to the magnetic permeability of its medium [34]. The physical properties of the medium are non-ferroelectric and non-ferromagnetic ignoring the Thompson influence. Maxwell's equations of electrodynamics for piezoelectric porous disk can be written as [35, 36]:

$$\underline{J} = \nabla \times \underline{v}, \qquad \nabla \times \underline{E} = -\mu \frac{\partial \underline{v}}{\partial t},$$

$$\nabla \bullet \underline{v} = 0, \qquad \underline{E} = -\mu \left( \frac{\partial \underline{u}}{\partial t} \times \underline{H} \right),$$

$$\underline{v} = \nabla \times (\underline{u} \times \underline{H}).$$

(9)

The initial magnetic vector $\underline{H} \equiv (0,0,H)$, the displacement vector $\underline{u} \equiv (u,0,0)$ and $\underline{v} \equiv (0,0,v)$ are all used in Eq. (9) to obtain:

$$\underline{E} = -\mu(r) \left( 0, H \frac{\partial u}{\partial t}, 0 \right),$$

$$\underline{J} = \left( 0, -\frac{\partial v}{\partial r}, 0 \right),$$

$$v = -H \left( \frac{\partial u}{\partial r} + \frac{2u}{r} \right),$$

(10)

where $H$ is a uniform magnetic field.

In what follows we assume that the elastic, piezoelectric, dielectric, pyroelectric, and thermal coefficients of the porous annular disk are subjected to the gradient relation (3). Now, let us consider the symmetry postulate in geometry and take into account the inertia and Lorentz force, the differential equation of motion of the porous FG disk written in the form:

$$\frac{d}{dr}(h(r)\sigma_r) + \frac{h(r)}{r}(\sigma_r - \sigma_\theta) + h(r)(F_r + F_H) = 0,$$

$$F_r = \rho \omega^2 r,$$

$$F_H = \mu(r)(\underline{J} \times \underline{H}) = H^2 \frac{\partial}{\partial r} \left( \mu \frac{du}{dr} + \mu \frac{nu}{r} \right),$$

(11)

where $F_r$, $F_H$ are the inertia and Lorentz forces, respectively, and Maxwell's equation can be expressed as:

$$\frac{d}{dr}(h(r)D_r) + \frac{h(r)}{r}D_r = 0,$$

(12)

in which $D_r$ gives the electric displacement.

## 4. Mathematical Solution Procedure for the Annular Disk with Porosity

The mathematical solution for the porous disk takes some steps, firstly find the electric displacement in equation (12), then solve the temperature equation (4) and substitute in the equation of motion (11). The solution of electric displacement of Eq. (12) are expressed as:

$$D_r = \frac{A_1}{r\,h(r)}$$

(13)

where $A_1$ is a constant of integration. By using equations (7), (13), and gradation relation (3), the electric potential functions yields:

$$\frac{d\psi}{dr} = \frac{1}{\varepsilon_{rr}} \left( e_{rr} \frac{du}{dr} + e_{r\theta} \frac{u}{r} + p_{11} T(r) - \frac{A_1}{r\,h(r)} \right),$$

(14)

Integrating again to get the electric potential function we gain a new integration constant $A_2$. By substituting into the differential motion equation (11) the value of the electric potential function (14), we get:

$$\frac{d^2 u}{dr^2} + \left( \frac{h(r)\frac{dm_{11}}{dr} + m_{11}\frac{dh(r)}{dr} + h(r)H^2\frac{d\mu}{dr}}{h(r)(m_{11}+\mu H^2)} + \frac{1}{r} \right) \frac{du}{dr} + \left( \frac{h(r)\frac{dm_{12}}{dr} + m_{12}\frac{dh(r)}{dr} + h(r)H^2\frac{d\mu}{dr}}{rh(r)(m_{11}+\mu H^2)} - \frac{m_{22}+\mu H^2}{r^2(m_{11}+\mu H^2)} \right) u,$$

$$+ \frac{m_{31}}{m_{11}+\mu H^2} \frac{dT}{dr} + \left( \frac{h(r)\frac{dm_{31}}{dr} + m_{31}\frac{dh(r)}{dr}}{h(r)(m_{11}+\mu H^2)} + \frac{m_{31}-m_{32}}{r(m_{11}+\mu H^2)} \right) T(r)$$

$$- \left( \frac{\frac{dm_{41}}{dr}}{rh(r)(m_{11}+\mu H^2)} - \frac{m_{42}}{r^2 h(r)(m_{11}+\mu H^2)} \right) A_1 + \frac{\rho \omega^2 r}{h(r)(m_{11}+\mu H^2)} = 0,$$

(15)

where $m_{ij}$ are functions of $r$:

$$\left. \begin{array}{c} m_{11} = c_{rr} + \dfrac{e_{rr}e_{rr}}{\varepsilon_{rr}}, \quad m_{12} = c_{r\theta} + \dfrac{e_{rr}e_{r\theta}}{\varepsilon_{rr}}, \quad m_{22} = c_{\theta\theta} + \dfrac{e_{r\theta}e_{r\theta}}{\varepsilon_{rr}}, \\[2mm] m_{31} = \dfrac{e_{rr}p_{11}}{\varepsilon_{rr}} - \lambda_r, \quad m_{32} = \dfrac{e_{r\theta}p_{11}}{\varepsilon_{rr}} - \lambda_\theta, \qquad m_{41} = \dfrac{e_{rr}}{\varepsilon_{rr}}, \\[2mm] m_{42} = \dfrac{e_{r\theta}}{\varepsilon_{rr}}, \end{array} \right\},$$

(16)

Postulate the mechanical and electric boundary conditions in this study in two examples as follows:

### 4.1 Circular annular disk (Free-Free)

$$\sigma_r|_{r=a} = -P_1, \quad \sigma_r|_{r=b} = -P_2, \quad \psi(r)|_{r=a} = \psi_1, \quad \psi(r)|_{r=b} = \psi_2,$$

(17)

### 4.2 Mounted annular disk (Fixed-Free)

$$u(r)|_{r=a} = 0, \quad \sigma_r|_{r=b} = -P_2, \quad \psi(r)|_{r=a} = \psi_1, \quad \psi(r)|_{r=b} = \psi_2,$$

(18)

where $P_i$, $\psi_i$ are the pressures and electric potentials on the internal and external radii of the disk, respectively.

To finish the mathematical solution for the annular porous disk, it is necessary to solve the heat equation (4) and the equilibrium equation (15), and both equations are functions in $r$, and it is very difficult to solve them in an analytical form. Therefore, it is appropriate in this case to use the semi-analytical technique to solve the two equations. In this technique, the radial domain is split into some virtual sections with a thickness $s^{(k)}$, as shown in Figure 4. The estimate of the factors of Eqs. (4) and (15) at $r = r^{(k)}$, the mean radius of the $k^{th}$ section, and utilizing them as appropriate variable coefficients in Eqs. (4) and (15), that is:

$$\frac{d^2 T(r^{(k)})}{dr^2} + G_1^{(k)} \frac{dT(r^{(k)})}{dr} = 0, \tag{19}$$

$$\frac{d^2 u^{(k)}}{dr^2} + N_1^{(k)} \frac{du^{(k)}}{dr} + N_2^{(k)} u^{(k)} + N_3^{(k)} = 0, \tag{20}$$

where,

$$G_1^{(k)} = \left. \left( \frac{1}{r} + \frac{\frac{dh(r)}{dr}}{h(r)} + \frac{\frac{dk_T(r)}{dr}}{k_T(r)} \right) \right|_{r=r^{(k)}}$$

$$N_1^{(k)} = \left. \frac{h(r)\frac{dm_{11}}{dr} + m_{11}\frac{dh(r)}{dr} + h(r)H^2\frac{d\mu}{dr}}{h(r)(m_{11}+\mu H^2)} \right|_{r=r^{(k)}} + \frac{1}{r^{(k)}},$$

$$N_2^{(k)} = \left. \frac{h(r)\frac{dm_{12}}{dr} + m_{12}\frac{dh(r)}{dr} + h(r)H^2\frac{d\mu}{dr}}{rh(r)(m_{11}+\mu H^2)} \right|_{r=r^{(k)}} - \left. \frac{m_{22}+\mu H^2}{r^2(m_{11}+\mu H^2)} \right|_{r=r^{(k)}}, \tag{21}$$

$$N_3^{(k)} = \left. \frac{m_{31}}{m_{11}+\mu H^2} \right|_{r=r^{(k)}} \left. \frac{dT}{dr} \right|_{r=r^{(k)}} + \left( \left. \frac{h(r)\frac{dm_{31}}{dr} + m_{31}\frac{dh(r)}{dr}}{h(r)(m_{11}+\mu H^2)} \right|_{r=r^{(k)}} + \left. \frac{m_{31}-m_{32}}{r(m_{11}+\mu H^2)} \right|_{r=r^{(k)}} \right) T(r^{(k)})$$

$$- \left( \left. \frac{\frac{dm_{A1}}{dr}}{rh(r)(m_{11}+\mu H^2)} \right|_{r=r^{(k)}} - \left. \frac{m_{42}}{r^2 h(r)(m_{11}+\mu H^2)} \right|_{r=r^{(k)}} \right) A_1^{(k)} + \left. \frac{\rho\omega^2 r}{h(r)(m_{11}+\mu H^2)} \right|_{r=r^{(k)}},$$

where $m_{ij}$ are functions of $r^{(k)}$. Using the semi-analytical solution of two differential equations (19), (20) with constant coefficients and $m$ is the number of hypothetical sections. Thus, the solution to the differential equations is:

$$T^{(k)} = C_1^{(k)} + C_2^{(k)} e^{-G_1^{(k)} r}, \tag{22}$$

$$u^{(k)} = B_1^{(k)} e^{\delta_1 r} + B_2^{(k)} e^{\delta_2 r} - \frac{N_3^{(k)}}{N_2^{(k)}} \tag{23}$$

where $\delta_1$, $\delta_2$ indicate algebraic roots of $\delta^2 + N_1^{(k)}\delta + N_2^{(k)} = 0$, and $C_1^{(k)}$, $C_2^{(k)}$, $B_1^{(k)}$, and $B_2^{(k)}$ are the differential equations constants for the $k^{th}$ section. The temperature solution (22) and the radial displacement (23) were verified for:

$$r^{(k)} - \frac{s^{(k)}}{2} \leq r \leq r^{(k)} + \frac{s^{(k)}}{2} \tag{24}$$

where $s^{(k)}$ and $r^{(k)}$ are the radial width and the mean radius of the $k^{th}$ section.

The temperature and radial displacement constants $C_1^{(k)}$, $C_2^{(k)}$, $B_1^{(k)}$, and $B_2^{(k)}$ determined from the continuity conditions between every two-adjacent sections. Thus, the continuity conditions for temperature, radial displacement, radial stress, and electric potential at the interfaces of the neighboring section are:

$$\left. \begin{array}{l} T^{(k)}\big|_{r=r^{(k)}+\frac{S^{(k)}}{2}} = T^{(k+1)}\big|_{r=r^{(k+1)}-\frac{S^{(k+1)}}{2}} \\[6pt] \frac{dT^{(k)}}{dr}\big|_{r=r^{(k)}+\frac{S^{(k)}}{2}} = \frac{dT^{(k+1)}}{dr}\big|_{r=r^{(k+1)}-\frac{S^{(k+1)}}{2}} \\[6pt] u^{(k)}\big|_{r=r^{(k)}+\frac{S^{(k)}}{2}} = u^{(k+1)}\big|_{r=r^{(k+1)}-\frac{S^{(k+1)}}{2}} \end{array} \right\}, \tag{25a}$$

$$\left. \begin{array}{l} \sigma_r^{(k)}\big|_{r=r^{(k)}+\frac{S^{(k)}}{2}} = \sigma_r^{(k+1)}\big|_{r=r^{(k+1)}-\frac{S^{(k+1)}}{2}} \\[6pt] \psi^{(k)}\big|_{r=r^{(k)}+\frac{S^{(k)}}{2}} = \psi^{(k+1)}\big|_{r=r^{(k+1)}-\frac{S^{(k+1)}}{2}} \\[6pt] \frac{d\psi^{(k)}}{dr}\big|_{r=r^{(k)}+\frac{S^{(k)}}{2}} = \frac{d\psi^{(k+1)}}{dr}\big|_{r=r^{(k+1)}-\frac{S^{(k+1)}}{2}} \end{array} \right\}, \tag{25b}$$
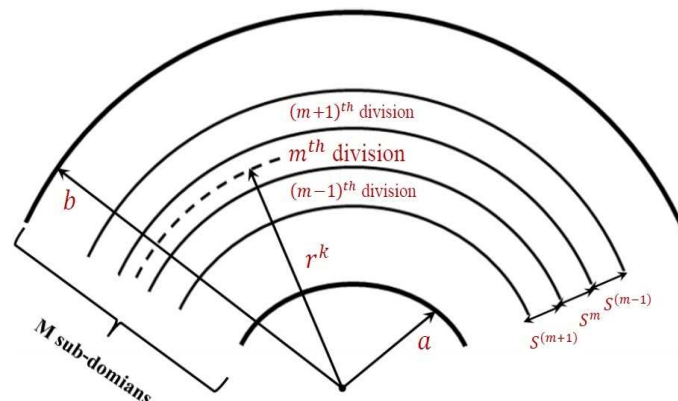


**Fig. 4.** Dividing a radial range into several hypothetical sections.

**Table 1.** Physical material coefficients for inner and outer materials.

| PZT-4 [25] | Cadmium selenide [26] |
|---|---|
| $c_{rr}^{(a)} = 115 \times 10^9$ (Pa) | $c_{rr}^{(b)} = 83.6 \times 10^9$ (Pa) |
| $c_{r\theta}^{(a)} = 74.3 \times 10^9$ (Pa) | $c_{r\theta}^{(b)} = 39.3 \times 10^9$ (Pa) |
| $c_{\theta\varphi}^{(a)} = 77.8 \times 10^9$ (Pa) | $c_{\theta\varphi}^{(b)} = 45.2 \times 10^9$ (Pa) |
| $c_{\theta\theta}^{(a)} = 139 \times 10^9$ (Pa) | $c_{\theta\theta}^{(b)} = 74.1 \times 10^9$ (Pa) |
| $e_{rr}^{(a)} = 15.1$ (Cm$^{-2}$) | $e_{rr}^{(b)} = 0.347$ (Cm$^{-2}$) |
| $e_{r\theta}^{(a)} = -5.2$ (Cm$^{-2}$) | $e_{r\theta}^{(b)} = 0.16$ (Cm$^{-2}$) |
| $\varepsilon_{rr}^{(a)} = 3.87 \times 10^{-9}$ (C$^2$K$^{-1}$m$^2$) | $\varepsilon_{rr}^{(b)} = 9.03 \times 10^{-11}$ (C$^2$K$^{-1}$m$^2$) |
| $p_{11}^{(a)} = -2.5 \times 10^{-5}$ (CK$^{-1}$m$^{-2}$) | $p_{11}^{(b)} = -2.94 \times 10^{-6}$ (CK$^{-1}$m$^{-2}$) |
| $K_T^{(a)} = 110$ (WK$^{-1}$m$^{-1}$) | $K_T^{(b)} = 4$ (WK$^{-1}$m$^{-1}$) |
| $\alpha_r^{(a)} = 2 \times 10^{-5}$ (K$^{-1}$) | $\alpha_r^{(b)} = 2.458 \times 10^{-6}$ (K$^{-1}$) |
| $\alpha_\theta^{(a)} = 2 \times 10^{-6}$ (K$^{-1}$) | $\alpha_\theta^{(b)} = 4.396 \times 10^{-6}$ (K$^{-1}$) |
| $\mu^{(a)} = 4\pi \times 10^{-7}$ (Hm$^{-1}$) | $\mu^{(b)} = 6.15 \times 10^{-5}$ (Hm$^{-1}$) |
| $\rho^{(a)} = 7500$ (kg m$^{-3}$) | $\rho^{(b)} = 5684$ (kg m$^{-3}$) |

**Table 2.** Comparison between perfect, even, and uneven porosity distribution in the circular annular disk.

| Variable | $\bar{r}$ | Perfect FGPM ($\beta = 0$) | | | Even FGPM ($\beta = 0.1$) | | | Uneven FGPM ($\beta = 0.1$) | | |
|---|---|---|---|---|---|---|---|---|---|---|
| | | $n=5$ | $n=10$ | $n=20$ | $n=5$ | $n=10$ | $n=20$ | $n=5$ | $n=10$ | $n=20$ |
| $\bar{u}$ | 0.3 | -0.1542 | -0.1714 | -0.1814 | -0.1529 | -0.1711 | -0.1806 | -0.5746 | -0.4012 | -0.2832 |
| | 0.5 | 0.2189 | 0.1729 | 0.1666 | 0.2196 | 0.1822 | 0.1671 | -1.1126 | -0.4196 | -0.0805 |
| | 0.7 | 0.2026 | 0.1484 | 0.1283 | 0.2034 | 0.1488 | 0.1294 | -2.2241 | -0.8388 | -0.2585 |
| $\bar{\sigma}_r$ | 0.3 | 1.3416 | 1.3042 | 1.2825 | 1.3425 | 1.3053 | 1.2993 | 0.6401 | 0.8627 | 1.0759 |
| | 0.5 | 0.7817 | 0.7428 | 0.7257 | 0.7842 | 0.7429 | 0.7258 | -0.7087 | 0.0614 | 0.4403 |
| | 0.7 | 0.5406 | 0.5107 | 0.4952 | 0.5443 | 0.5129 | 0.4978 | -1.4917 | -0.3618 | 0.1432 |
| $\bar{\sigma}_\theta$ | 0.3 | 0.5515 | 0.5653 | 0.5677 | 0.5369 | 0.5513 | 0.5537 | 1.3351 | 0.8538 | 0.6675 |
| | 0.5 | 0.2824 | 0.3072 | 0.3082 | 0.2676 | 0.2929 | 0.2936 | 1.9754 | 0.8938 | 0.5033 |
| | 0.7 | 0.2104 | 0.2347 | 0.2316 | 0.2019 | 0.2262 | 0.2224 | 2.1697 | 0.8781 | 0.4343 |
| $\bar{\psi}$ | 0.3 | 3.5225 | 3.4828 | 3.4333 | 3.7515 | 3.6986 | 3.6442 | 3.3999 | 3.0721 | 3.4391 |
| | 0.5 | 3.0959 | 3.0146 | 2.9623 | 3.2661 | 3.1707 | 3.1143 | 2.0164 | 2.1801 | 2.5762 |
| | 0.7 | 3.0697 | 2.9337 | 2.8702 | 3.2095 | 3.05819 | 2.9915 | -1.2336 | 0.8828 | 2.0296 |
| $\bar{T}$ | 0.3 | 1.0248 | 1.0305 | 1.0349 | 1.0254 | 1.0312 | 1.0357 | 1.0025 | 1.0198 | 1.0303 |
| | 0.5 | 1.0621 | 1.0762 | 1.0872 | 1.0631 | 1.0775 | 1.0886 | 1.0063 | 1.0496 | 1.0761 |
| | 0.7 | 1.0972 | 1.1178 | 1.1348 | 1.0985 | 1.1193 | 1.1363 | 1.0099 | 1.0771 | 1.1181 |

The continuity relations (25) jointly with circular annular disk conditions Eq. (17) or with mounted annular disk Eq. (18) yield linear equations system in constants $A_1^{(k)}$, $A_2^{(k)}$, $B_1^{(k)}$, $B_2^{(k)}$, $C_1^{(k)}$, $C_2^{(k)}$, $(k = 1,2,\ldots,m)$. After solving the linear system, the temperature $T^{(k)}$ and radial displacement $u^{(k)}$ is specified in each section. For better results accuracy, increase the number of hypothetical divisions.

## 5. Numerical Outcomes

The numerical outcomes of even and uneven porosity distribution on FG annular disks with variable thickness are investigated. The hollow disk is conducting with PZT-4 on the inner surface and Cadmium selenide on the outer ones. The physical coefficients of the inner (PZT-4) and outer (Cadmium Selenide) surfaces are recorded in Table 1. The material coefficients obey a power function in the radial direction. Different thickness description is considered in Figures (1) and (2). Suppose that in the annular disk $b = 5a$ and the disk is subjected to several loading. Mechanical, thermal, and magneto-electric loads occur. Two examples are studied, namely circular annular disk and mounted annular disk.

### 5.1 Circular annular disk (Free-Free)

Assume that a power thickness description with concave profiles achieves equation (1) by $l = 0.415196$, $k = 3$. The thermal, mechanical, and electric boundary conditions on the form:

$$\left.\begin{aligned}
T(r)|_{r=a} = T_0 = 298 \text{ (K)}, \quad & T(r)|_{r=b} = T_1 = 373 \text{ (K)}, \\
\sigma_r|_{r=a} = -pb = -10^{10} \text{ (Pa)}, \quad & \sigma_r|_{r=b} = 0 \text{ (Pa)}, \\
\psi|_{r=a} = \psi_0 = 10^8 \text{ (W/A)}, \quad & \psi|_{r=a} = 0 \text{ (W/A)}.
\end{aligned}\right\} \tag{26}$$

### 5.2 Mounted annular disk (Fixed-Free)

Suppose an exponential disk profile with a convex shape obeys the relation (2) by $l = 2$, $k = 0.5$. The loading boundary conditions of this case are:

$$\left.\begin{aligned}
T(r)|_{r=a} = T_0 = 298 \text{ (K)}, \quad & T(r)|_{r=b} = T_1 = 373 \text{ (K)}, \\
u|_{r=a} = 0 \text{ (m)}, \quad & \sigma_r|_{r=b} = -pb = -10^{10} \text{ (Pa)}, \\
\psi|_{r=a} = 0 \text{ (W/A)}, \quad & \psi|_{r=a} = \psi_0 = 10^8 \text{ (W/A)}.
\end{aligned}\right\} \tag{27}$$

Consider the dimensionless form:

$$\left.\begin{aligned}
\bar{r} = \frac{r}{b}, \quad & \bar{u} = \frac{u}{b} \times 10^2, \quad & \bar{T}(\bar{r}) = \frac{T(\bar{r})}{T_0}, \\
\bar{\psi}(\bar{r}) = \frac{\psi(\bar{r})}{\psi_0}, \quad & \bar{h}(\bar{r}) = \frac{h(\bar{r})}{h_0}, \quad & \bar{\sigma}_i(\bar{r}) = \frac{\sigma_i(\bar{r})}{pb}, \quad (i = r, \theta).
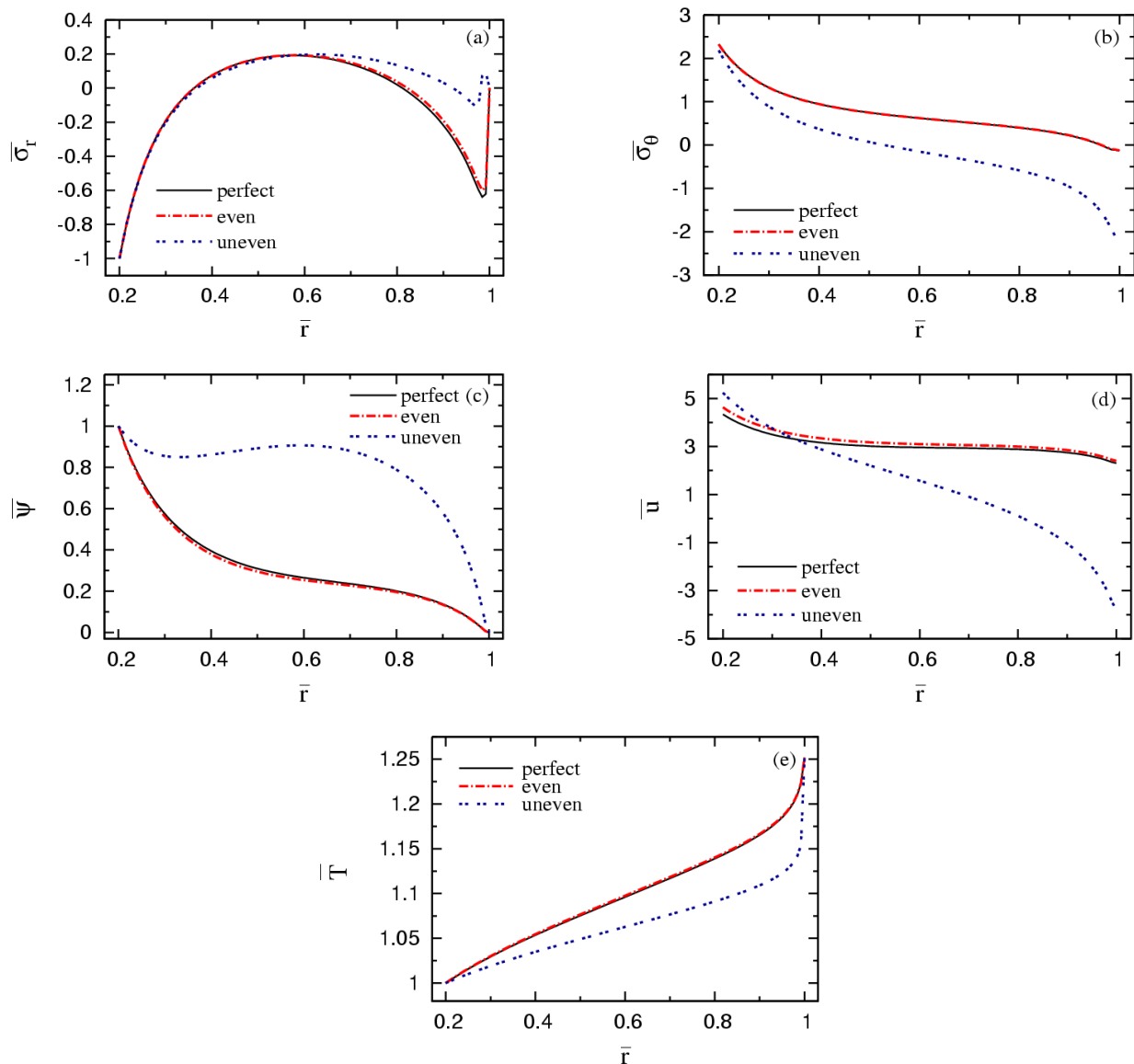\end{aligned}\right\} \tag{28}$$

**Fig. 5.** Comparison between stresses, electric potential, radial displacement, and temperature in the circular porous annular disk.

## 6. Validation

### 6.1 Circular annular disk (Free-Free)

The comparison between the circular annular disk made of perfect material and the disk made of porous material with even or uneven porosity distribution is presented in Table 2 and Figure 5. It is clear from the data and graphics that the values of radial stress, hoop stress, radial displacement, and temperature in even porosity distribution are higher than that of perfect material or uneven porosity distribution at different positions and multiple values of grading index $n$. While the electric potential function in uneven porosity distribution achieved the highest values.

### 6.2 Mounted annular disk (Fixed-Free)

The case of a mounted annular disk is illustrated in Table 3 and Figure 6. It can be concluded from the numerical values in the table and graph that the highest value of radial and hoop stresses was achieved in perfect materials for several values of grading index $n$ and several positions, while radial displacement and temperature occurred the highest value in even porosity distribution. Whereas in uneven porosity distribution, the electric potential functions reached the highest values.

### 6.3 Circular annular disk (Free-Free)

Stresses, electric potential, radial displacement, and temperature are studied for even and uneven porosity distribution, respectively for various values of grading index $n$ and porosity factor $\beta = 0.1$ in Figures 7 and 8. Figure 7 appears the effect of grading index $n$ in the case of even porosity. Figure 7(a) presents the radial stress; all curves satisfy the mechanical boundary conditions on the inner and outer surfaces with several values of $n$. Hoop stress is illustrated in Figure 7(b). The curves are decreases from the inner to outer surfaces for all values of grading index $n$.

From Figure 7(c) the electric potential is equal to one on the inner surface and equal to zero on the outer ones. From the graph, the electric potential function decreases along the radial direction. Figure 7(d) demonstrates the radial displacement. The highest values occur at $n \to \infty$ and the lowest values happen at $n = 20$. All curves are decreased from internal to external surfaces. Figure 7(e) displays the temperature-graded curves. The figure presents all curves obeying the temperature boundary conditions. It is clear that the temperature value is increase with the increase in the grading index $n$.

**Table 3.** Comparison between perfect, even, and uneven porosity distribution in the mounted annular disk.

| Variable | $\bar{r}$ | Perfect FGPM ($\beta = 0$) | | | Even FGPM ($\beta = 0.1$) | | | Uneven FGPM ($\beta = 0.1$) | | |
|---|---|---|---|---|---|---|---|---|---|---|
| | | $n = 5$ | $n = 10$ | $n = 20$ | $n = 5$ | $n = 10$ | $n = 20$ | $n = 5$ | $n = 10$ | $n = 20$ |
| $\bar{u}$ | 0.3 | 0.9281 | 0.9313 | 0.9352 | 0.8957 | 0.8989 | 0.9046 | 0.1009 | 0.5055 | 0.7435 |
| | 0.5 | 0.5961 | 0.6118 | 0.6367 | 0.5703 | 0.5857 | 0.6124 | -1.6764 | -0.3218 | 0.2824 |
| | 0.7 | 0.1661 | 0.1798 | 0.2181 | 0.1484 | 0.1623 | 0.2024 | -3.3145 | -1.1283 | -0.2454 |
| $\bar{\sigma}_r$ | 0.3 | 0.1929 | 0.2129 | 0.2419 | 0.1859 | 0.2062 | 0.2368 | -1.9634 | -0.6119 | -0.0579 |
| | 0.5 | 0.2553 | 0.2768 | 0.3112 | 0.2409 | 0.2624 | 0.2988 | -2.3718 | -0.7374 | -0.0553 |
| | 0.7 | 0.1434 | 0.1562 | 0.1951 | 0.1295 | 0.1425 | 0.1834 | -2.9319 | -1.0235 | -0.2228 |
| $\bar{\sigma}_\theta$ | 0.3 | 0.4443 | 0.4313 | 0.4121 | 0.4468 | 0.4332 | 0.4134 | 1.5674 | 0.7961 | 0.5249 |
| | 0.5 | 0.9714 | 0.9461 | 0.9087 | 0.9753 | 0.9489 | 0.9105 | 3.0654 | 1.6064 | 1.1074 |
| | 0.7 | 1.2496 | 1.2193 | 1.1763 | 1.2525 | 1.2209 | 1.1769 | 3.4423 | 1.8804 | 1.3651 |
| $\bar{\psi}$ | 0.3 | 0.3965 | 0.4094 | 0.4278 | 0.4041 | 0.4178 | 0.4386 | -1.1066 | -0.1889 | -0.2046 |
| | 0.5 | 0.9384 | 0.9776 | 1.0358 | 0.9396 | 0.9809 | 1.0458 | -3.7729 | -0.8677 | 0.3662 |
| | 0.7 | 1.1841 | 1.2374 | 1.6425 | 1.1869 | 1.2395 | 1.6457 | -7.5609 | -2.1062 | 0.1529 |
| $\bar{T}$ | 0.3 | 1.0276 | 1.0332 | 1.0373 | 1.0282 | 1.0339 | 1.0381 | 1.0033 | 1.0229 | 1.0331 |
| | 0.5 | 1.0709 | 1.0853 | 1.0958 | 1.0722 | 1.0867 | 1.0972 | 1.0084 | 1.0591 | 1.0854 |
| | 0.7 | 1.1108 | 1.1314 | 1.1474 | 1.1121 | 1.1328 | 1.1489 | 1.0132 | 1.0914 | 1.1321 |
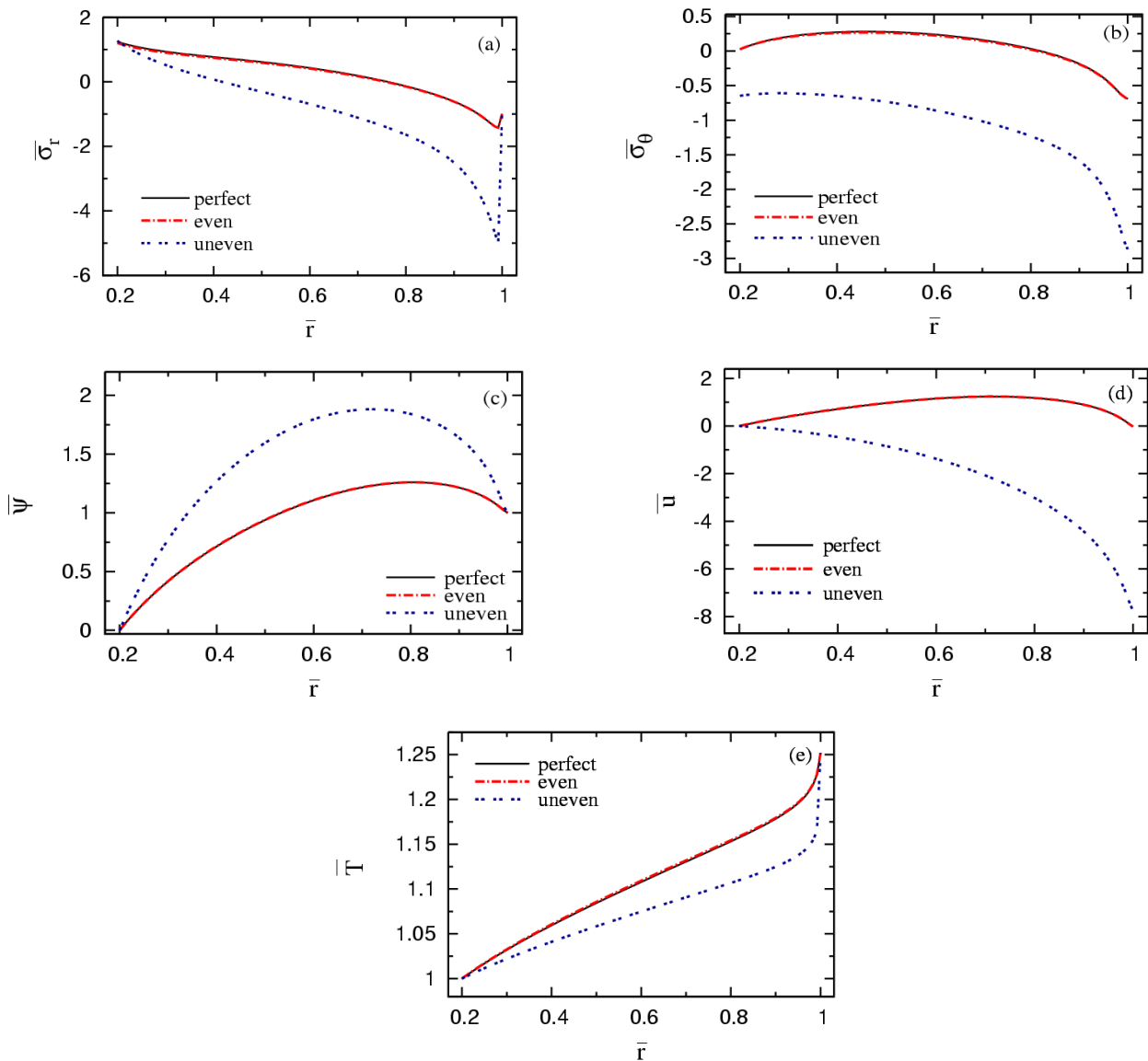


**Fig. 6.** Comparison between stresses, electric potential, radial displacement, and temperature in the mounted porous annular disk.

Figure 8 shows the results in the case of uneven porosity distribution for various grading index values $n$. Figure (8) presents the radial stress for multiple values of $n$. All curves decrease along the disk radius and then increase nearby the outer surface to satisfy the mechanical boundary condition. Hoop stress is displayed in Figure 8(b). The lowest value of stress achieves at $n = 5$ and then the hoop stress increase with the increase of grading index $n$. The curves are decreases from the inner to the outer surfaces. Figure 8(c) appears the electric potential function with different $n$ values. All curves are intersecting at the same point at the inner and outer radius to obey the electric boundary conditions. The radial displacement presents in Figure 8(d). The graded curves intersect at $\bar{r} = 0.44$. The radial displacement decreases with increases in the grading index value after the intersection. Figure 8(e) illustrates the temperature-graded curves. The value of graded curves increases by increasing the grading index $n$.

Figures 9 and 10 show the effect of the porosity parameter on the annular disk in the case of even and uneven distributions, respectively with porosity parameter values $\beta = 0.2,\ 0.4,\ 0.6$. Figure 9(a) displays the radial stress. Notices that all curves are semi-coincide with several values of porosity parameter $\beta$. The hoop stress is shown in Figure 9(b). Also, the curves are semi-coincide from the inner to the outer surfaces. Figure 9(c) demonstrates the electric potential function. It is appearing the influence of the porosity parameter. The value of the electric potential function is increased by decreasing the value of the porosity parameter. Figure 9(d) clearly shows the influence of porosity parameter $\beta$ on the radial displacement. The radial displacement values are increased by increasing the porosity parameter values. Figure 9(e) presents the temperature distribution by multiple values of the porosity parameter. The effect of porosity on temperature is shown in a direct relation as the increase in the porosity parameter value increases the temperature.

Figure 10 displays the study results in the uneven porosity distribution case. Figure 10(a) presents the radial stress and the influence of the porosity parameter at $\beta = 0.2, 0.4, 0.6$. Observes that increasing the porosity parameter means decreasing the radial stress. As well as the relation with hoop stress appears in Figure 10(b). The electric potential diagram appears in Figure 10(c). All curves with the change of porosity parameter values are semi-identical. The radial displacement is illustrated in Figure 10(d). All curves with the change of porosity parameter are intersected at $\bar{r} = 0.55$ and the curves changed their behavior. The temperature graph is presented in Figure 10(e). The increase in the porosity parameter value causes a decrease in the temperature value in the interval $0.2 \leq \bar{r} < 0.9$ and vice versa in the interval $0.9 \leq \bar{r} \leq 1$.
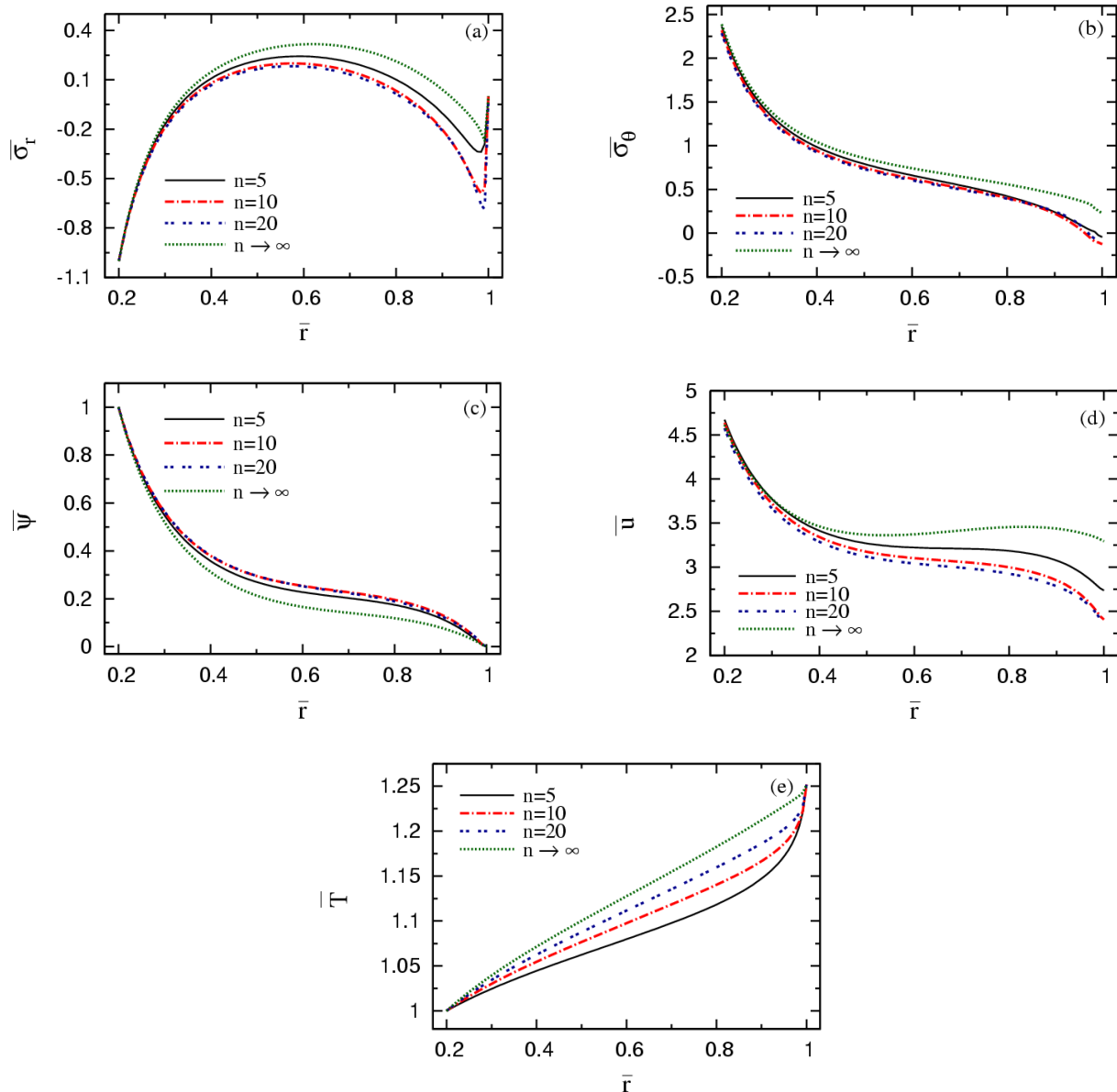


**Fig. 7.** Stresses, electric potential, radial displacement, and temperature with various values of grading index in circular annular disk with even porosity distribution and porosity parameter $\beta = 0.1$.
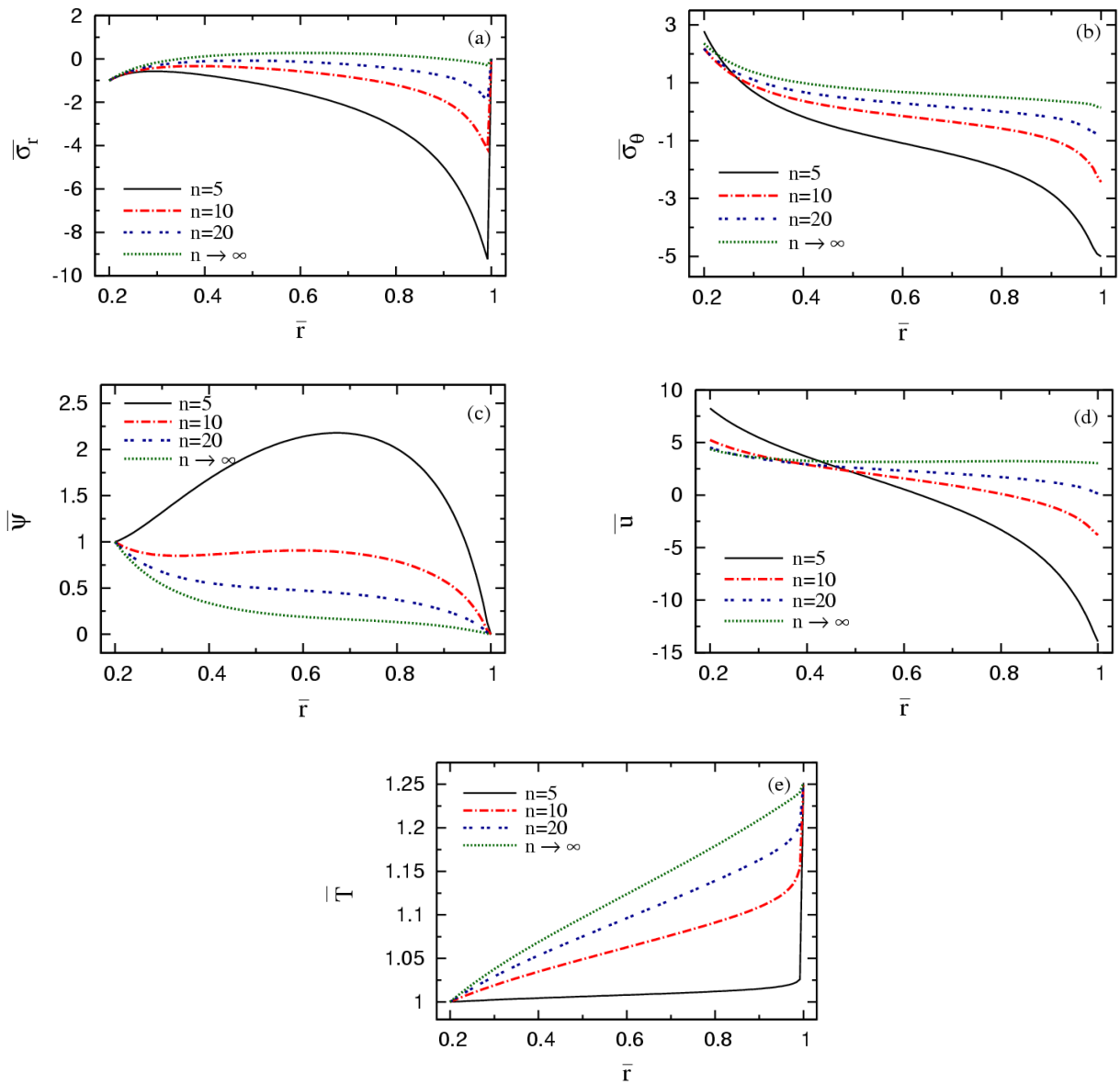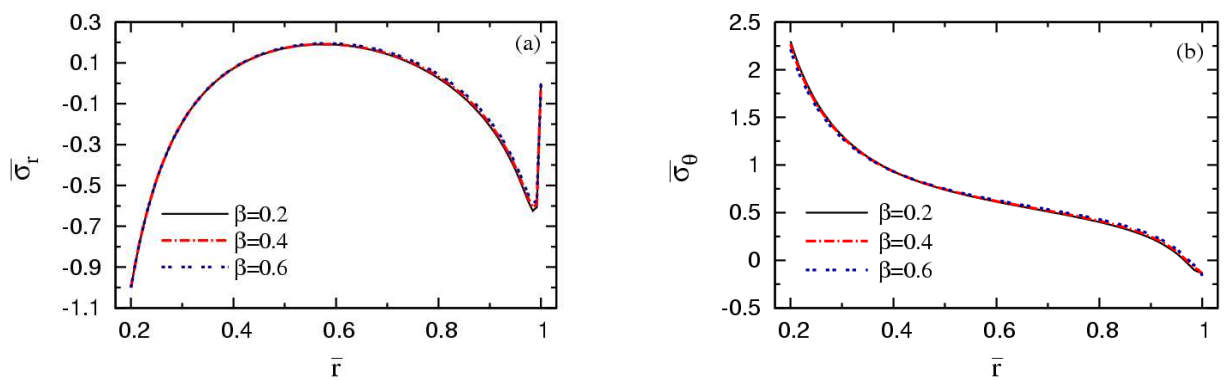
**Fig. 8.** Stresses, electric potential, radial displacement, and temperature with various values of grading index in circular annular disk with uneven porosity distribution and porosity parameter $\beta = 0.1$.



**Fig. 9.** Influence of porosity parameter on stresses, electric potential, radial displacement, and temperature in a circular annular disk with even porosity distribution and grading index $n = 12$.
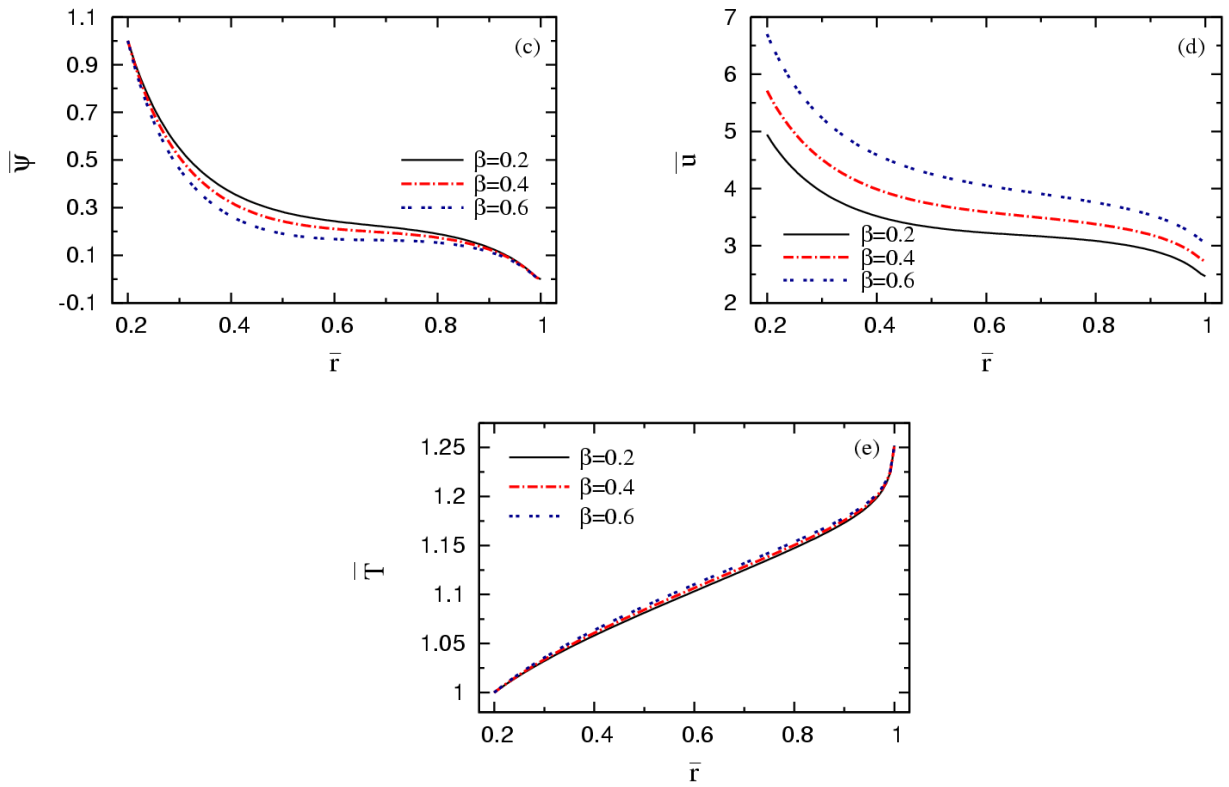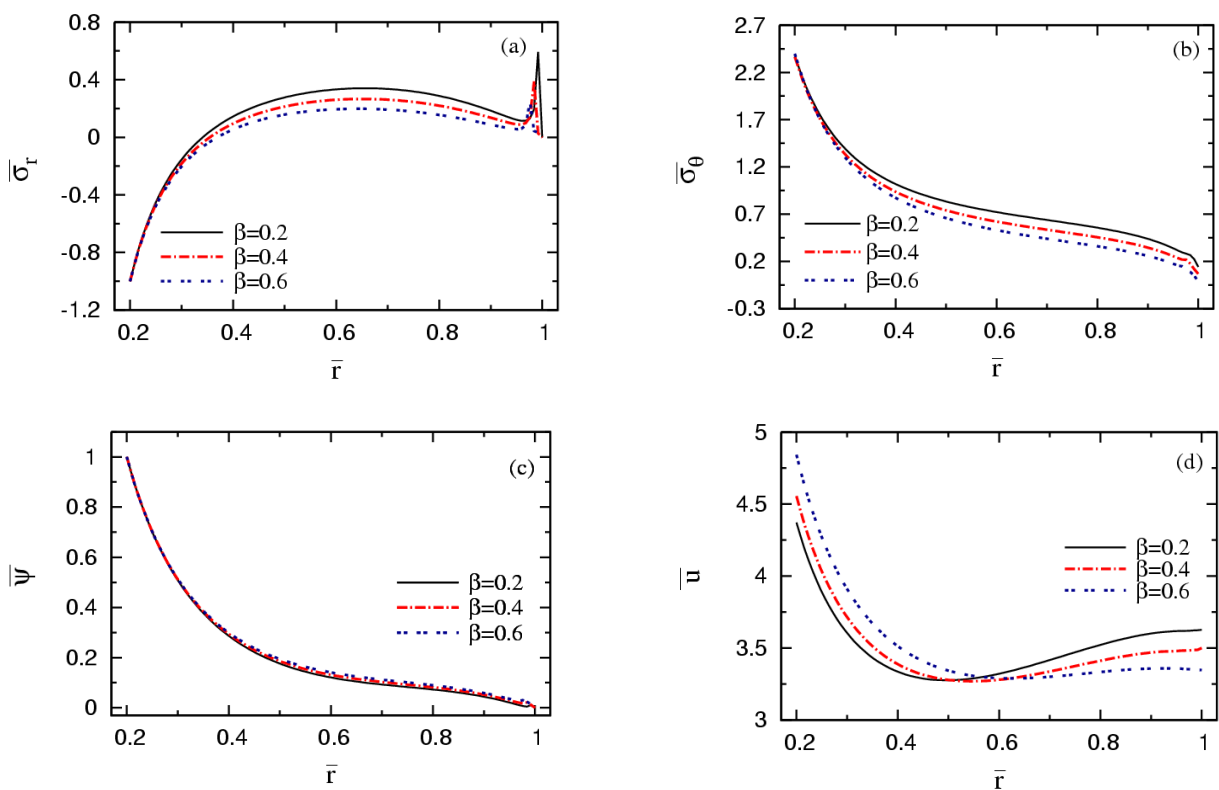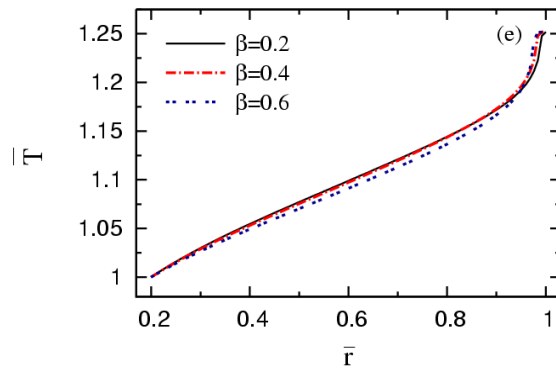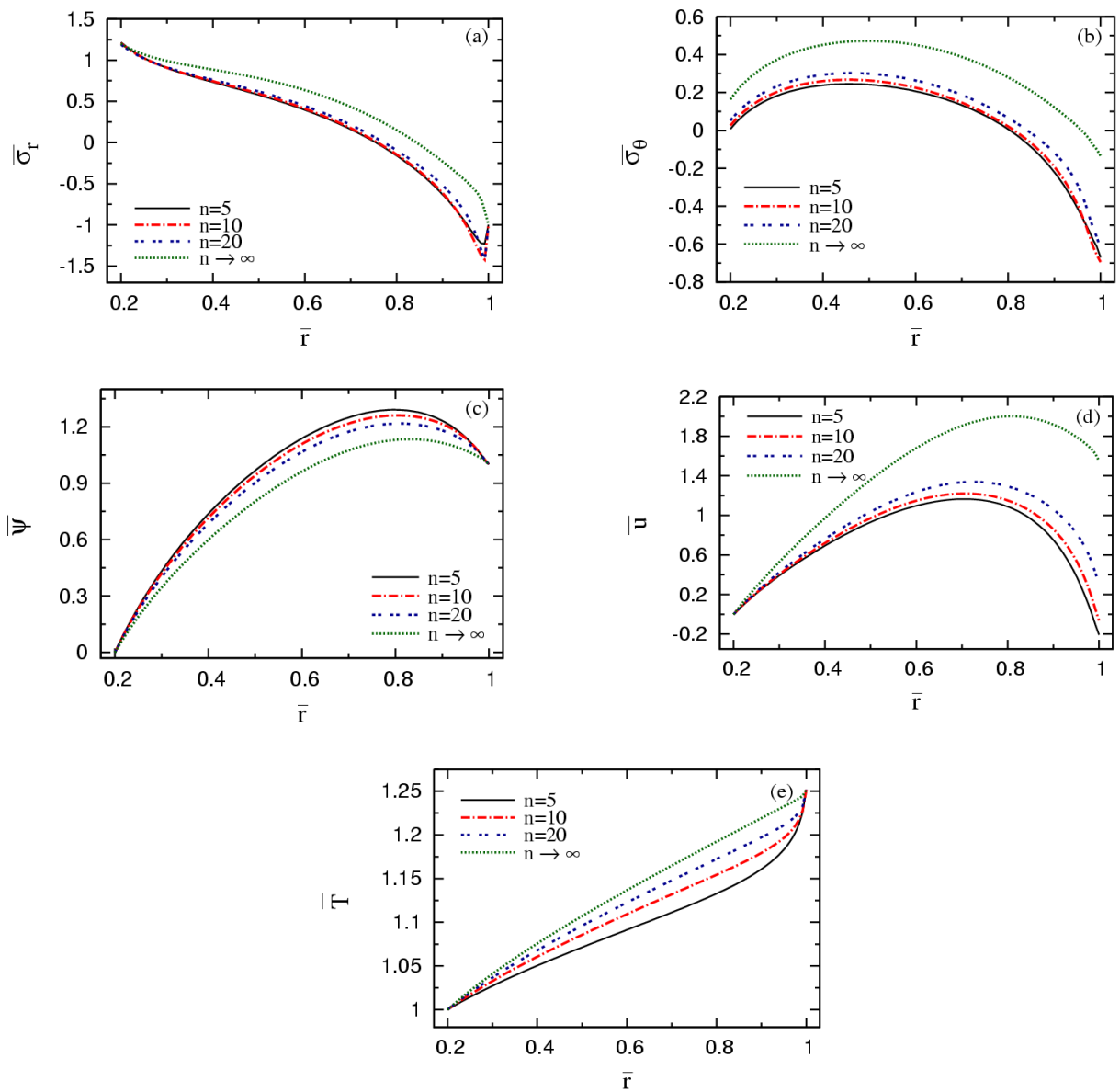
**Fig. 9.** Continued.



**Fig. 10.** Influence of porosity parameter on stresses, electric potential, radial displacement, and temperature in a circular annular disk with uneven porosity distribution and grading index $n = 12$.
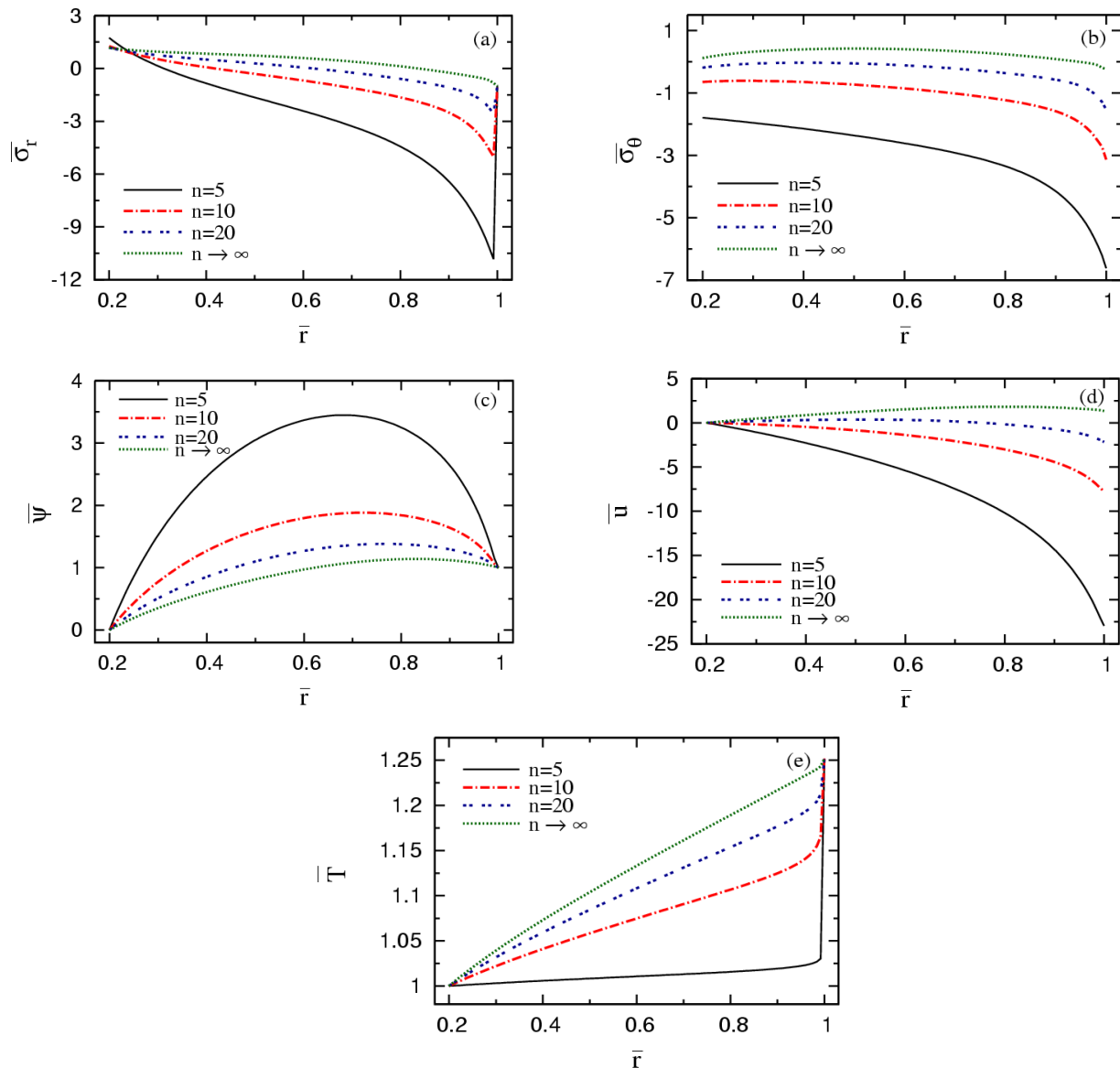
**Fig. 10.** Continued.



**Fig. 11.** Stresses, electric potential, radial displacement, and temperature with various values of grading index in mounted annular disk with even porosity distribution and porosity parameter $\beta = 0.1$.

**Fig. 12.** Stresses, electric potential, radial displacement, and temperature with various values of grading index in mounted annular disk with uneven porosity distribution and porosity parameter $\beta = 0.1$.

### 6.4 Mounted annular disk (Fixed-Free)

Figures 11 and 12 offer the numerical result of the study in the case of the mounted annular disk with the change of grading index parameter in even and uneven porosity distribution, respectively. Figure 11(a) shows the radial stress with radial direction. The radial stress curves are decreases along the radial direction and then increase nearby the outer radius to satisfy the mechanical boundary conditions. While Figure 11(b) presents the hoop stress with several values of grading index. The hoop stress increases to its maximum value then it decreases when $\bar{r} = 0.6$ up to the outer radius. In Figure 11(c) the influence of the grading index is clearly shown. All curves are increases and decrease near the outer surface to obey the electric boundary conditions. The higher grading index value means a lower electric potential function value. The radial displacement presents in Figure 11(d). The radial displacement is increasing and decreases at $\bar{r} = 0.8$ to the outer surface. The lower value of radial displacement curves occurs at $n = 5$ and the higher value happens at $n \to \infty$. Figure 11(e) displays the temperature gradient with multiple values of grading index $n$. The higher value of temperature occurs with the higher value of grading index $n$.

Figure 12(a) presents the radial displacement with several values of grading index $n$. The radial stress decreases and then increases nearby the external surface to satisfy the boundary conditions. The radial stress and grading index are in extreme relation. Figure 12(b) displays the hoop stress with various values of grading index $n$. by increasing the value of $n$ the hoop stress increases. An electric potential function satisfying the electric boundary conditions in Figure 12(c). By increasing the grading index $n$ the value of the electric potential function decreases. The radial displacement appears in Figure 12(d). The displacement equals zero at the inner surface, and this agrees with mechanical boundary conditions. There is extreme relation between grading index $n$ and temperature. The lower value of temperature achieves at $n = 5$ while the higher value occurs at $n \to \infty$.

The effect of porosity parameters on stresses, electric potential function, radial displacement, and temperature offers in Figures 13 and 14 for even and uneven porosity distributions, respectively. Figure 13(a) presents the radial stress with different values of porosity parameter $\beta = 0.2, 0.4, 0.6$. With increases in the porosity factor $\beta$ the radial stress decreases. The same behavior of hoop stress is appeared in Figure 13(b) with porosity factor. In Figure 13(c), the curves of the electric potential function are semi-coincide together by different values of porosity factor $\beta$. Figure 13(d) displays the radial displacement with the porosity parameter. There is extreme relation between radial displacement and porosity parameters up to $\bar{r} = 0.55$, then the relationship turns to an inverse

relation until the outer surface. Also, the extreme relation between temperature and porosity parameter appears in Figure 13(e).

For uneven porosity distribution, figure 14 displays the results. There is extreme relation between the radial stress and porosity factor up to $\bar{r} = 0.75$ then the behavior changes, this is clear in Figure 14(a). The same behavior of hoop stress Figure 14(b), but the change of behavior occurs at $\bar{r} = 0.95$. Figure 14(c) demonstrates the extreme relation between the electric potential function and porosity parameter along the radial direction. While the radial displacement is in an inverse relation with the porosity parameter, in Figure 14(d). Figure 14(e) presents the temperature gradient with several porosity parameter values. All curves are semi-coincide with each other.
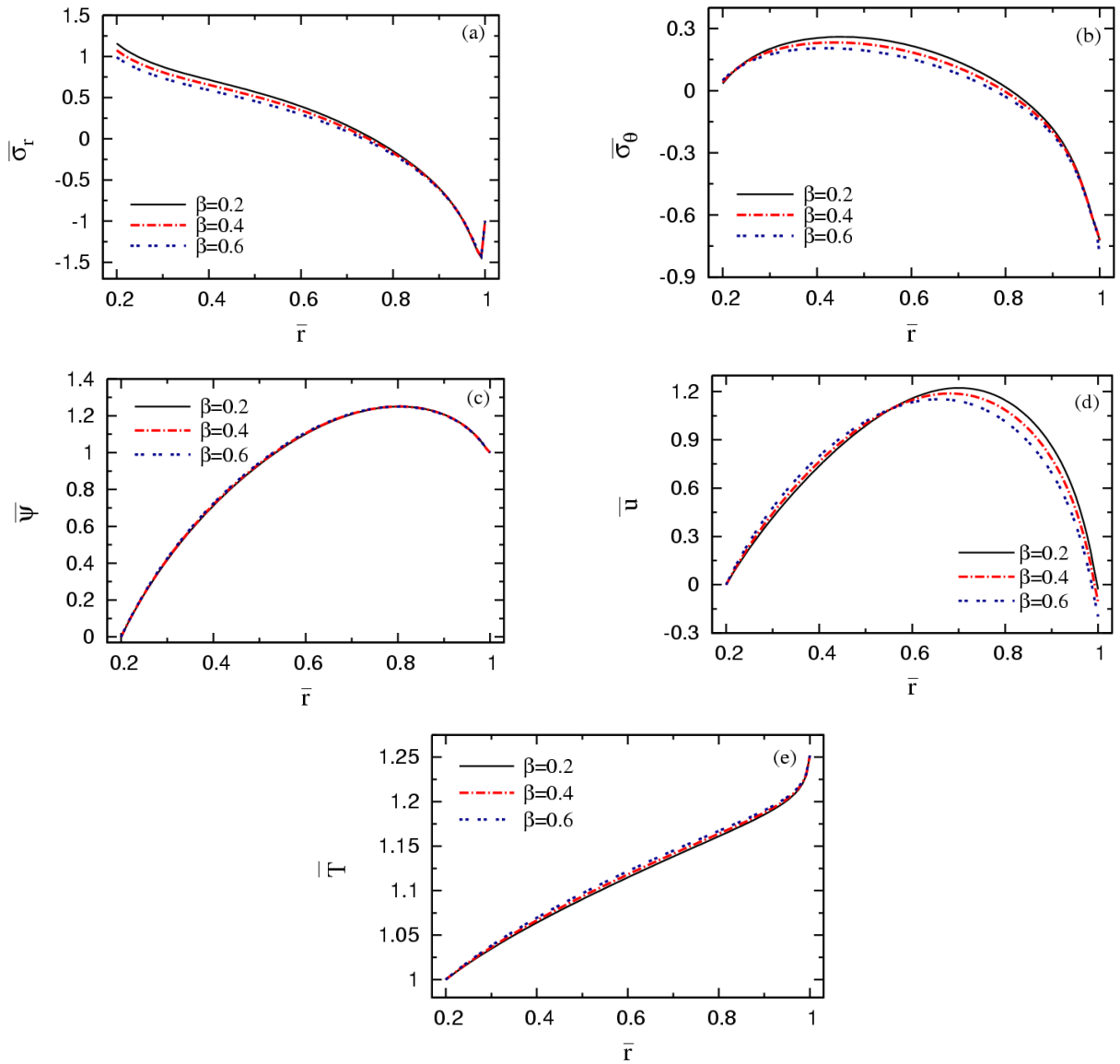


**Fig. 13.** Influence of porosity parameter on stresses, electric potential, radial displacement, and temperature in mounted annular disk with even porosity distribution and grading index $n = 12$.
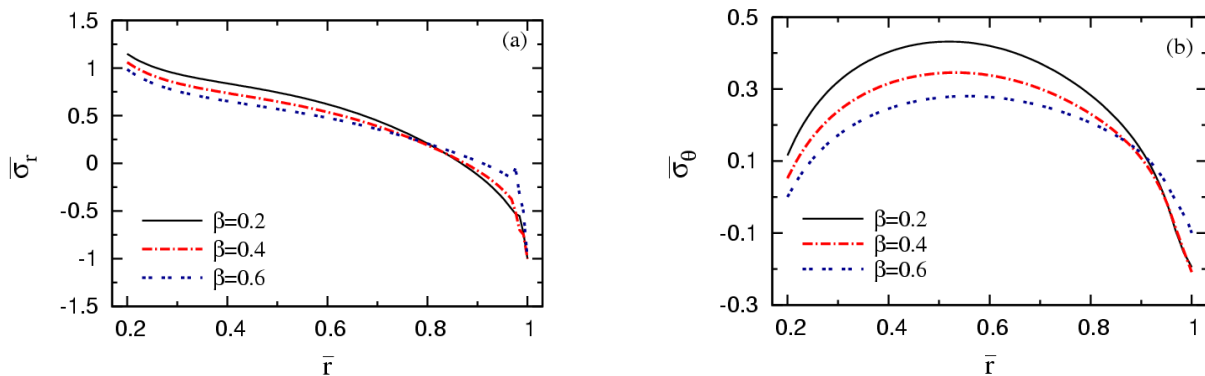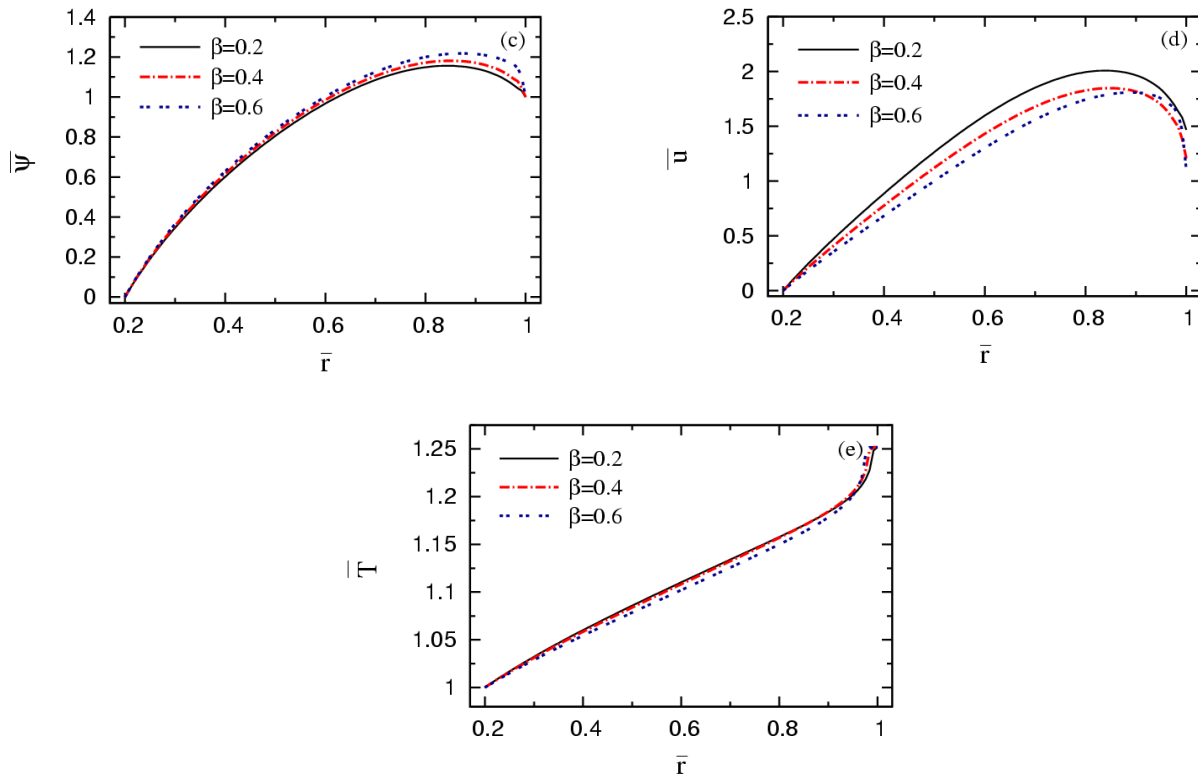


**Fig. 14.** Influence of porosity parameter on stresses, electric potential, radial displacement, and temperature in mounted annular disk with uneven porosity distribution and grading index $n = 12$.

**Fig. 14.** Continued.

## 7. Conclusions

In this paper, the porosity in the form of two different distributions, even and uneven porosity distributions, was studied in an annular disk of variable thickness rotating with constant angular velocity. The disk was affected by mechanical, electrical, and magnetic forces, in addition to the thermal effect. All physical parameters of the disk were subject to power relation in the radial direction. The porous disk was studied using two sets of boundary conditions of a circular annular and a mounted annular disk. To obtain the temperature and radial displacement, the semi-analytical technique was used. After a comparison between the non-porous material and the porous one under the influence of even and uneven porosity distribution, the following conclusions are drawn:

- For circular annular disk: stresses, radial displacement, and temperature achieves the higher value in the case of even porosity distribution, while the electric potential function occurs the highest value in the uneven porosity distribution.
- For mounted annular disk: the stresses achieve a higher value in nonporous (perfect) material. The higher value of radial displacement and temperature occurs in an even porosity distribution and the electric potential function occurs higher in the uneven porosity distribution.
- The importance of choosing suitable values for grading index and porosity parameter in porous materials were demonstrated to design an engineering model and obtain specific values of stresses and displacements.

## Author Contributions

The authors initiated the manuscript and suggested the mathematical technique. The article was written through the contributions of two authors. They examined the results, revised and confirmed the final version of the paper.

## Conflict of Interest

The authors confirmed no conflict of interest.

## Data Availability Statements

The data used in the research is available by corresponding author upon reasonable request for scientific research.

## Nomenclature

| | | | |
|---|---|---|---|
| $a$ | Inner radii of the annular disk [m] | $\alpha_i \ (i = r, \theta)$ | Thermal expansion coefficients [K$^{-1}$] |
| $b$ | Outer radii of the annular disk [m] | $\beta$ | A porosity volume function |
| $c_{ij} \ (i = r, \theta, j = r, \theta, \varphi)$ | Elastic coefficients [Pa] | $D_r$ | Electric displacement |
| $e_{rj} \ (j = r, \theta)$ | Piezoelectric parameters [C m$^{-2}$] | $\varepsilon_{rr}$ | Dielectric parameters [C$^2$K$^{-1}$m$^2$] |
| $H$ | Uniform magnetic field [kg $C^{-1}$ sec$^{-1}$] | $h(r)$ | The variable thickness of the rotating disk profile [m] |
| $h_0$ | Thickness at the axis of the disk [m] | $\psi$ | Electric potential distribution [$W/A$] |
| $K_T$ | Thermal conductivity [W/K m] | $\mu(r)$ | Magnetic permeability [Hm$^{-1}$] |
| $n$ | Grading index | $l, k$ | Dimensionless geometric parameter |
| $\omega$ | Angular velocity | $r^{(k)}$ | Mean radius of the kth subdomain [m] |
| $s^{(k)}$ | The radial width of the kth division [m] | $\sigma_r$ | Radial stress distribution [Pa] |
| $\sigma_\theta$ | Circumferential stress distribution [Pa] | $T(r)$ | Temperature distribution [K] |
| $T_0$ | Reference initial temperature [K] | $\rho$ | The density of the material [kg m$^{-3}$] |
| $p_a$ | Properties of the inner surface | $p_b$ | Properties of the outer surface |
| $p_{11}$ | Pyroelectric coefficients [CK$^{-1}$m$^{-2}$] | $P_1$ | Inner pressure [Pa] |
| $P_2$ | Outer pressure [Pa] | $u(r)$ | Radial displacement [m] |

## References

[1] Abazid, M.A., Zenkour, A.M., Sobhy, M., Wave propagation in FG porous GPLs-reinforced nanoplates under in-plane mechanical load and Lorentz magnetic force via a new quasi 3D plate theory, *Mechanics Based Design of Structures and Machines*, 50(5), 2022, 1831-1850.

[2] Ebrahimi, F., Jafari, A., Barati, M.R., Vibration analysis of magneto-electro-elastic heterogeneous porous material plates resting on elastic foundations, *Thin-Walled Structures*, 119, 2017, 33–46.

[3] Arefi, M., Firouzeh, S., Rezaei Bidgoli, E.M., Civalek, O., Analysis of porous micro-plates reinforced with FG-GNPs based on Reddy plate theory, *Composite Structures*, 247, 2020, 112391.

[4] Barati, M.R., Shahverdi, H., Aero-hygro-thermal stability analysis of higher-order refined supersonic FGM panels with even and uneven porosity distributions, *Journal of Fluids and Structures*, 73, 2017, 125–136.

[5] Sobhy, M., Zenkour, A.M., Wave propagation in magnetoporosity FG bi-layer nanoplates based on a novel quasi-3D refined plate theory, *Waves in Random and Complex Media*, 31(5), 2021, 921-941.

[6] Vaka, V., Sathujoda, P., Bhalla, N. A., Kumar, Y.V.S., Steady-state and transient vibration analysis of a thermally loaded power law-based functionally graded rotor system with induced porosities, *Forces in Mechanics*, 9, 2022, 100123.

[7] Kumar, R., Panchal, M., Elastodynamic response of vibrations in a magneto-micropolar porous medium possessing cubic symmetry, *Chemical Engineering Communications*, 197, 2010, 1500–1514.

[8] Kumar, R., Sharma, P., Variational principle, uniqueness and reciprocity theorems in porous magneto-piezothermoelastic medium, *Cogent Mathematics*, 3, 2016, 1231947.

[9] Karami, B., Shahsavari, D., Li, L., Temperature-dependent flexural wave propagation in nanoplatetype porous heterogenous material subjected to in-plane magnetic field, *Journal of Thermal Stresses*, 41(4), 2018, 483–499.

[10] Kiran, M.C., Kattimani, S.C., Vinyas, M., Porosity influence on structural behaviour of skew functionally graded magneto-electro-elastic plate, *Composite Structures*, 191, 2018, 36–77.

[11] Wattanasakulpong, N., Ungbhakorn, V., Linear and nonlinear vibration analysis of elastically restrained ends FGM beams with porosities, *Aerospace Science and Technology*, 32 (1), 2014, 111–120.

[12] Akbas, S., Thermal Effects on the Vibration of Functionally Graded Deep Beams with Porosity, *International Journal of Applied Mechanics*, 9(5), 2017, 1750076.

[13] Chen, D., Kitipornchai, S., Yang, J., Nonlinear free vibration of shear deformable sandwich beam with a functionally graded porous core, *Thin-Walled Structures*, 107, 2016, 39-48.

[14] Ebrahimi, F., Jafari, A., A higher-order thermomechanical vibration analysis of temperature-dependent FGM beams with porosities, *Journal of Engineering*, 2016, 2016, 9561504.

[15] Tantawy, R., Zenkour, A.M. Effect of Porosity and Hygrothermal Environment on FGP Hollow Spheres under Electromechanical Loads, *Journal of Applied and Computational Mechanics*, 8(2), 2022, 710–722.

[16] Zenkour, A.M., Quasi-3D refined theory for functionally graded porous plates: displacements and stresses, *Physical Mesomechanics*, 23(1), 2020, 22-35.

[17] Mashat, D.S., Zenkour, A.M., Radwan, A.F., Aquasi – 3D higher order plate theory for bending of FG plates resting on elastic foundations under hygro-thermo-mechanical loads with porosity, *European Journal of Mechanics/ A Solids*, 82, 2020, 103985.

[18] Qing, H., Wei, L., Linear and nonlinear free vibration analysis of functionally graded porous nanobeam using stress-driven nonlocal integral model, *Communications in Nonlinear Science and Numerical Simulation*, 109, 2022, 106300.

[19] Tang, Y., Qing, H., Size-dependent nonlinear post-buckling analysis of functionally graded porous Timoshenko microbeam with nonlocal integral models, *Communications in Nonlinear Science and Numerical Simulation*, 116, 2023, 106808.

[20] Zhao, Y., Zhang, S., Wang, X., Ma, S., Zhao, G., Kang, Z., Nonlinear analysis of carbon nanotube reinforced functionally graded plates with magneto-electro-elastic multiphase matrix, *Composite Structures*, 297, 2022, 115969.

[21] Zhang, S., Zhao, Y., Wang, X., Chen, M., Schmidt, R., Static and dynamic analysis of functionally graded magneto-electro-elastic plates and shells, *Composite Structures*, 281, 2022, 114950.

[22] Zhang, S., Huang, Z., Zhao, Y., Ying, S., Ma, S., Static and dynamic analyses of FGPM cylindrical shells with quadratic thermal gradient distribution, *Composite Structures*, 277, 2021, 114658.

[23] Wei, L., Qing, H., Bending, buckling and vibration analysis of Bi-directional functionally graded circulary annular microplate based on MCST, *Composite Structures*, 292, 2022, 115633.

[24] Shariati, M., Shishehsaz, M., Mosalmani, R., Roknizadeh, S.A.S., Size effect on the axisymmetric vibrational response of functionally graded circular nano-plate based on the nonlocal stress-Driven method, *Journal of Applied and Computational Mechanics*, 8(3), 2022, 962-980.

[25] Ootao, Y., Tanigawa, Y., Transient piezothermoelastic analysis for a functionally graded thermopiezoelectric hollow sphere, *Composite Structures*, 81, 2007, 540–549.

[26] Arani, A.G., Kolahchi, R., Mosallaie Barzoki, A.A., Loghman, A., Electro-thermo-mechanical behaviors of FGPM spheres using analytical method and ANSYS software, *Applied Mathematical Modelling*, 36, 2012, 139–157.

[27] Bayat, M., Saleem, M., Sahari, B.B., Hamouda, A.M.S., and Mahdi, E., Mechanical and thermal stresses in a functionally graded rotating disk with variable thickness due to radially symmetry loads, *International Journal of Pressure Vessels and Piping*, 86, 2009, 357-372.

[28] Allam, M.N.M., Tantawy, R., Zenkour, A., Thermoelastic stresses in functionally graded rotating annular disks with variable thickness, *Journal of Theoretical and Applied Mechanics*, 56(4), 2018, 1029-1041.

[29] Bayat, M., Rahimi, M., Saleem, M., Mohazzab, A.H., Wudtke, I., Talebi, H., One dimensional analysis for magneto-thermo-mechanical response in a

functionally graded annular variable-thickness rotating disk, *Applied Mathematical Modelling*, 38(19), 2014, 4625-4639.

[30] Paria, G., Magneto-elasticity and magneto-thermo-elasticity, *Advances in Applied Mechanics*, 10(1), 1967, 73-112.

[31] Dai, T., Dai, H.L., Analysis of a rotating FGMEE circular disk with variable thickness under thermal environment, *Applied Mathematical Modelling*, 45, 2017, 900-924.

[32] Dai, H.L., Jiang, H.J., Analytical study for electromagnetothermoelastic behavior of a functionally graded piezoelectric solid cylinder, *Mechanics of Advanced Materials and Structures*, 20(10), 2013, 800-811.

[33] Dai, H.L., Dai, T., Yang, L., Free vibration of a FGPM circular plate placed in a uniform magnetic field, *Meccanica*, 48(10), 2013, 2339-2347.

[34] Ezzat, M.A., Generation of generalized thermomagnetoelastic waves by thermal shock in a perfectly conducting half-space, *Journal of Thermal Stresses*, 20, 1997, 633-917.

[35] Kraus, J.D., *Electromagnetic*, McGraw Hill, USA, 1984.

[36] Dai, H.L., Wang, X., Dynamic responses of piezoelectric hollow cylinders in an axial magnetic field, *International Journal of Solids and Structures*, 41, 2004, 5231-5246.

## ORCID iD

Rania Tantawy　https://orcid.org/0000-0002-0576-2798

Ashraf M. Zenkour　https://orcid.org/0000-0002-0883-8073

**Publisher's Note** Shahid Chamran University of Ahvaz remains neutral with regard to jurisdictional claims in published maps and institutional affiliations.